Metal-Only Monolithic 4x4 Horn Array Difference Pattern Antenna

José Rico-Fernández*, Álvaro F. Vaquero†, Marcos R. Pino†, Manuel Arrebola†
pepe.rico@northern-waves.com, fernandezvalvaro@uniovi.es, mpino@uniovi.es, arrebola@uniovi.es
*Northern Waves AB, Stockholm, Sweden
†Dept. of Electrical Engineering, Group of TSC, Universidad de Oviedo, Gijón, Spain,

***Abstract*—Additive Manufacturing Laser Powder-Bed Fusion (AM LPBF) technique is evaluated to manufacture monolithic antennas in metal, simplifying the conventional procedure based on, first, manufacturing a dielectric skeleton, and then, applying a coating process to obtain the desire microwave component. To validate the technique, a difference pattern array of 4×4 horn antennas is designed to operate at mm-wave frequencies. The antenna is based on a complex structure to obtain a difference radiation pattern by rotating twisted section in two different orientations. The prototype is manufactured in a monolithic piece of aluminum alloy AlSi10Mg, providing a single structure that includes both radiating elements and feeding network, including twisters and power dividers in waveguide. The prototype is evaluated in anechoic chamber and planar near-field scanner, obtaining a good agreement with full-wave simulations within the operational bandwidth (34 to 36 GHz). The experimental validation demonstrates that the technique LPBF is a suitable candidate to produce monolithic metal-only microwave components in the K_a band.**

I. Introduction

Differential pattern antennas serve crucial roles across a spectrum of applications where discerning signals from various directions is paramount. In radar systems, these antennas facilitate precise target tracking, like aircraft, ships, or weather phenomena, by analyzing phase and amplitude disparities among signals received by array elements [1]. Likewise, in wireless communication systems, particularly those employing beamforming or MIMO techniques, differential pattern antennas enhance signal reception and transmission efficacy by directing beams towards desired directions while mitigating interference. In radio astronomy, they enable the capture and analysis of celestial signals, aiding astronomers in deciphering properties of celestial objects through meticulous measurement of signal disparities across the antenna array. Moreover, in direction-finding systems, these antennas are pivotal for navigation, search and rescue operations, and military endeavors, as they enable determination of signal source directions by comparing signals received across the array. These versatile antennas thus play integral roles in a diverse array of applications requiring precise signal discernment and analysis.

Additive Manufacturing (AM) has emerged as an alternative to traditional manufacturing methods, like CNC milling, offering speed, precision, and cost benefits [2]. AM's ability to create complex geometries has attracted interest beyond mechanical engineering, notably in microwave engineering. Three methodologies dominate AM in antenna and microwave device fabrication: using plastic/dielectric materials for graded-index lenses [3]–[5], metasurfaces [6], and transmitarrays [7]–[9]; plastic components with metallic coatings like nickel [10], [11] or copper [12]–[15]; and metal-only AM techniques such as Laser Powder Bed Fusion (LPBF), ideal for space applications due to dielectric loss-free properties [10]–[15]. LPBF, involving layers of metal powder melted by a laser, produces lightweight, monolithic microwave components like waveguide filters, horn arrays, and shaped parallel plate lenses [16]–[20]. These advancements address alignment issues encountered in milling processes [21].

II. Antenna Design

The design of the horn array with difference pattern starts from an input port in rectangular waveguide WR28. This input port undergoes narrows down to achieve a more compact design and have good matching in the design band. This input port continues towards a power divider 1:2 in H-plane, using a septum for impedance matching. Again, each of the outputs of this 1:2 divider are concatenated by another 1:2 divider using the same topology. This achieves linear division 1:4 in the H-plane.

However, to achieve a planar array, a square aperture is required, with the same number of elements in the vertical and horizontal planes. Given the flexibility that additive manufacturing allows, it was decided to use 90° twist sections that allow changing from the H-plane to the E-plane. Specifically, if this twist is applied to two elements with clockwise orientation and two with counterclockwise orientation, a phase distribution with 180° phase difference is achieved. Furthermore, this plane change has the particularity and benefit of being able to reuse the same H-plane divider used in the input port. For the aperture, four 1:4 dividers have been stacked, each connected to a set of four rectangular to square horns. Figure 1 shows an exploded view of the horn array design with difference pattern, featuring two twisted

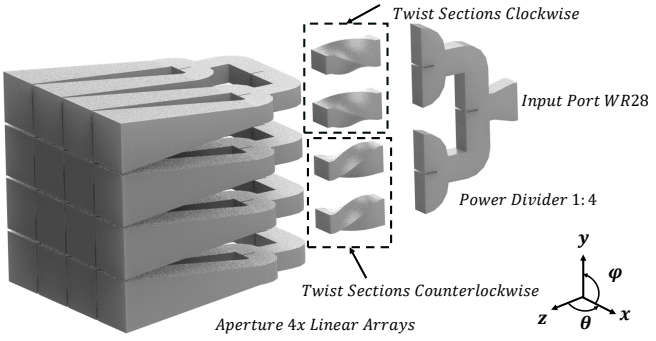

Fig. 1: Exploded view of difference pattern horn array design.

sections in clockwise orientation and two in counterclockwise orientation.

For the mechanical design of the differential pattern horn array, once again, thanks to the manufacturing possibilities, an envelope conforming to the vacuum design was created. This envelope typically has a thickness of 1.5 mm.

III. Manufacturing Process using Laser Powder Bed Fusion

To validate the design of the proposed monolithic horn array difference pattern antenna, incorporating various components such as waveguides, power dividers, twisters, and horn antennas, the decision was made to manufacture and test the aggregate version. AM LPBF technology was employed for fabrication, involving the deposition of metal powder layer-by-layer on a build plate, followed by selective melting using a laser beam as a heat source to achieve the desired structure. The resulting monolithic piece integrates the horn antenna array with the feeding network, utilizing solely aluminum alloy AlSi10Mg, with an electrical conductivity of $\sigma = 1.68 \times 10^7$ S/m [22]. This method eliminates the need for subsequent assembly and coating steps, streamlining production from two or three steps to just one, thereby reducing assembly errors and enhancing device performance. Post-processing of the prototype involves removing fabrication supports, sandblasting the outer surface, and machining the flanges for improved interface contact. The complexity of the design, including twisted sections, is challenging to produce via traditional methods, particularly when difference pattern antennas, where phase distribution along the aperture of the component is a critical aspect. Since LPBF was chosen from the beginning, the antenna design was tailored to accommodate process constraints. For instance, mechanical surfaces in the 4×4 horn antenna array were designed with no inclination exceeding 45° to align with manufacturing capabilities. Additionally, managing high temperatures during production is critical to prevent thermal deformations that could impact electromagnetic response. Thermal optimization was employed during cooling using multiple thicknesses to mitigate potential deformations.

For the manufacturing of the monolithic component, the printing direction followed the orientation of the z-axis with a rotation of 45°, as depicted in Fig. 1, with the flange placed against the building plate and the aperture positioned at the top. This orientation offers the advantage of design symmetry relative to the printing bed and reducing the need for supports during fabrication. Additionally, due to the design of the horn array, there are no areas presenting overhanging challenges.

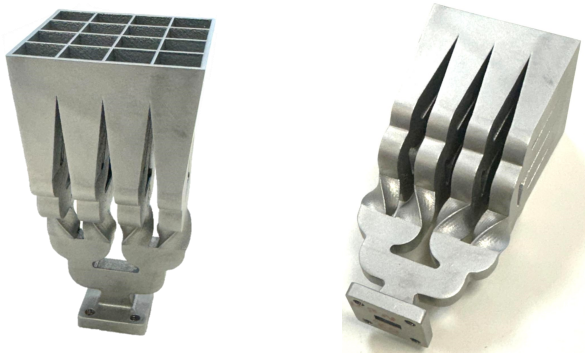

Fig. 2: Photographs of the addivitely manufactured difference pattern horn array antenna in AlSi10Mg.

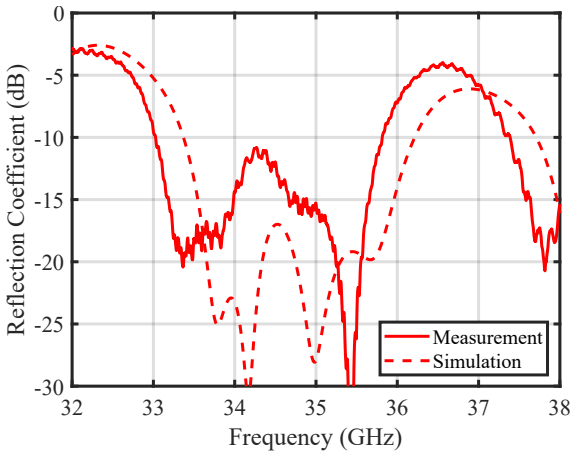

Fig. 3: Scattering parameters of difference pattern horn array prototype, comparing measured (*solid lines*) with simulated (*dashed lines*) results.

After manufacturing the monolithic piece using aluminum alloy AlSi10Mg, post-processing steps were initiated. Initially, the piece was detached from the printing bed along with the manufacturing supports. Subsequently, the supports were removed, and the piece underwent thorough cleaning. To further refine the surface, sandblasting was performed using glass microspheres. Finally, a machining cut was applied to the flange area, where an additional thickness of 500 μm had been incorporated to ensure proper contact with the measuring equipment. Overall, a surface roughness of 5-6 μm as-built is expected, and it is reduced down to 3-4 μm after sandblasting. In Fig.2, it is depicted a photograph of the additively manufactured difference pattern horn array antenna in aluminum alloy AlSi10Mg.

IV. Measurements

The prototype of difference pattern horn array antenna, manufactured using additive techniques, underwent measurement and experimental validation at the University of Oviedo, Spain. Initially, the reflection coefficient was assessed using the Agilent N5247A PNA-X vector analyzer to ensure proper functionality. The reflection coefficient compared with simulation is depicted in Fig. 3. The maximum measured reflection coefficient is -10.8 dB, compared with a maximum value of -17 dB in the simulation. Despite minor variations, primarily due to manufacturing tolerances, the measured results, below -10 dB closely align with simulated data, validating the performance of the device in the design frequency band.

Once the reflection coefficient was successfully validated, radiation pattern measurements were carried out. Firstly, the prototype of the difference pattern horn array was placed in the anechoic chamber (spherical range) of the University of Oviedo, Spain. In Fig. 4a an image of the measurement setup for the anechoic chamber is depicted. The normalized radiation patterns for the primary planes ($\phi = 0°$ and $\phi = 90°$) at 34 GHz are illustrated in Fig. 5 for both copolar (CO) and cross-polar (CX) Linear Polarized (LP) field components. It

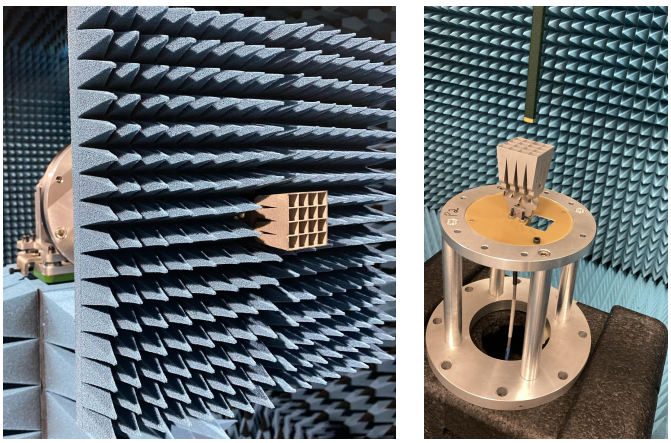

(a) (b)

Fig. 4: Measurement setup for the horn array additively manufactured prototype in (a) spherical range in anechoic chamber and (b) planar acquisition range.

is also presented a comparison from a full-wave numerical simulation, performed in CST Microwave Studio [23], with measurements in Fig. 5, showing an excellent agreement. Dashed lines for $\phi = 0°$, dotted lines for $\phi = 90°$ and solid lines for simulations.

The measured level for the null of the co-polarized component with respect to the maximum is -27 dB at 36 GHz, with SLLs remaining below -10 dB. It is important to note the frequency squint that happens around the center of the pattern due to electrical dimensions. Additionally, it is also presented in Fig. 6 the measured normalized radiation pattern for CO in the U-V plane at 34, 35 and 36 GHz respectively compared with simulations.

Furthermore, the prototype was also measured in the planar acquisition range in the University of Oviedo, Spain. A picture in Fig. 4b illustrates the prototype of the difference pattern horn array antenna mounted in the measurement setup in a planar acquisition range in semianechoic environment. The setup is comprised of an open-ended waveguide in the Ka-band used as near-field probe. Both probe and the prototype

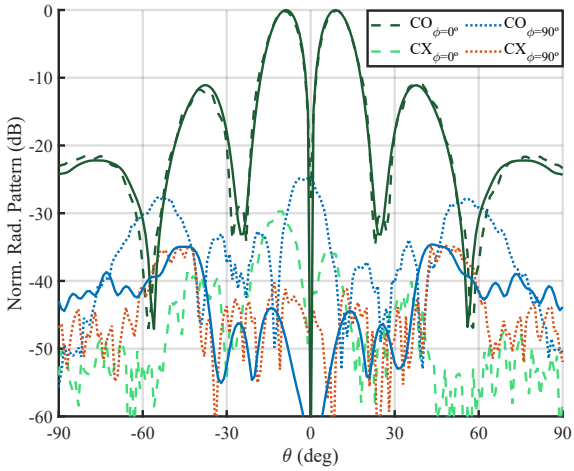

Fig. 5: Normalized radiation patterns of difference pattern horn array prototype at 34 GHz, comparing measured (*dashed and dotted lines*) with simulated (*solid lines*) results.

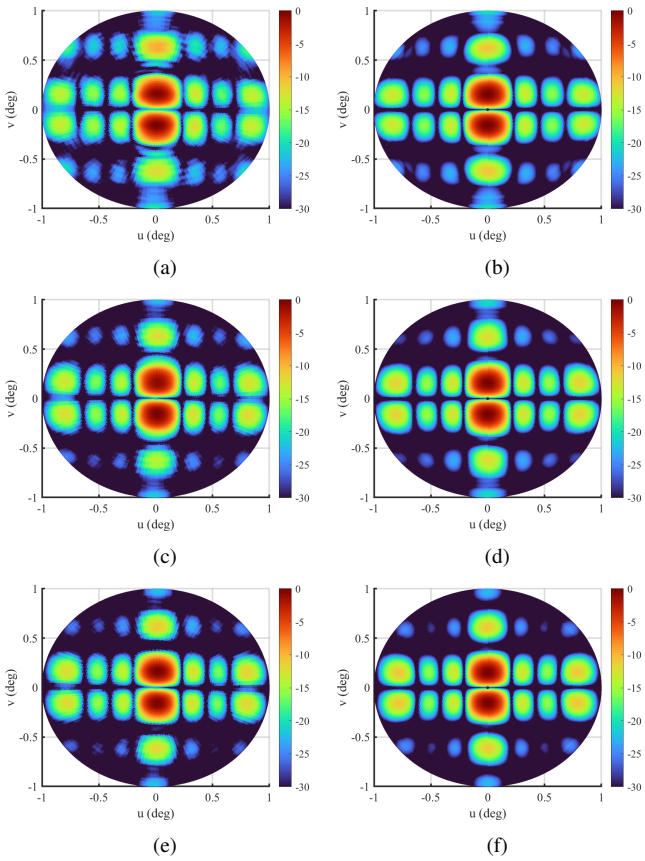

Fig. 6: U-V Normalized radiation patterns of the difference pattern horn array for (a) measurements at 34 GHz, (b) simulations at 34 GHz, (c) measurements at 35 GHz, (d) simulations at 35 GHz, (e) measurements at 36 GHz and (f) simulations at 36 GHz.

are connected to the Agilent N5247A PNA-X vector analyzer. Then a $100\times100\,\text{mm}^2$ plane is measured at 95 mm from the center of the antenna to get most of the radiated power. The grid is sampled each mm from 32 to 38 GHz. This measurement campaign is used to evaluate the phase difference in the aperture.

In Fig. 7, near-field measurements are illustrated, both in amplitude and phase, for frequencies of 34, 35, and 36 GHz. Remarkably, in Fig. 7a, 7c and 7e, amplitudes are shown with a null in the central part for the z-cut corresponding to the center of the aperture. Furthermore, in Fig. 7b, 7d and 7f, it is clearly observed how the upper part of the aperture, i.e., the linear arrays with counterclockwise twists, exhibit a phase difference of 180° compared to the lower part of the aperture, corresponding to the sections with clockwise twists, confirming the correct design and operation of the difference pattern.

Acknowledgement

This work was supported in part by MCIN/AEI/10.13039/501100011033 under Projects PID2020-114172RB-C21 and TED2021-130650B-C22, cofunded by European Union (EU) "NextGenerationEU"/PRTR; and in part by the Spanish Ministry of Universities and EU (NextGenerationEU/PRTR) under Grant MU-21-UP2021-03071895621J

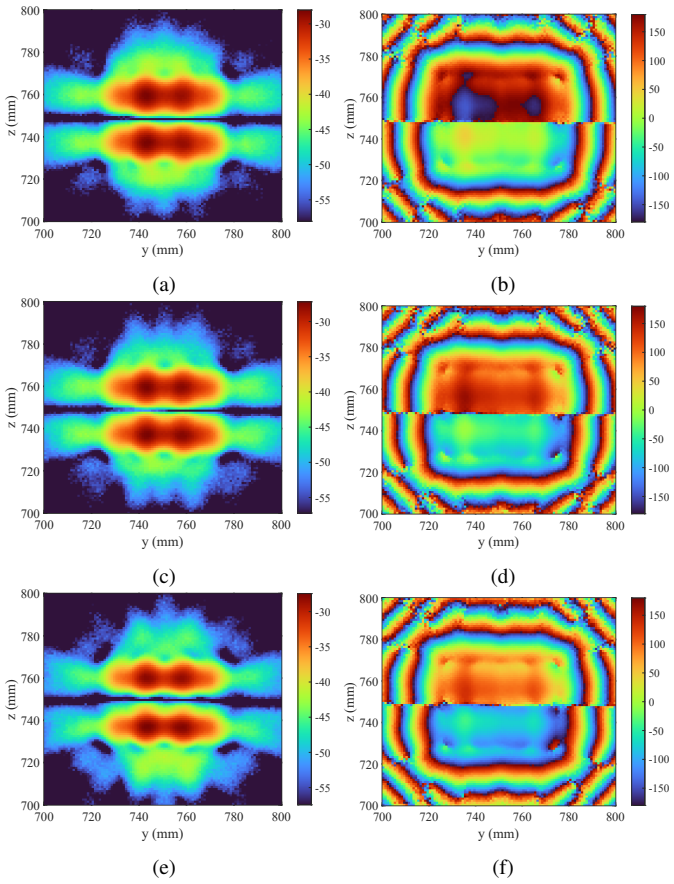

Fig. 7: Near-field measurements of difference pattern horn array prototype: (a) Amplitude at 34 GHz, (b) Phase at 34 GHz, (c) Amplitude at 35 GHz, (b) Phase at 35 GHz and (a) Amplitude at 36 GHz, (b) Phase at 36 GHz.

V. Conclusion

This paper presented a difference pattern horn array antenna experimentally validated by means of additive manufacturing technique LPBF. The manufacturing of a monolithic component allows to reduce misalignment errors and leakage, while giving the freedom of using only H-plane power dividers, thanks to the twist sections. Overall, a good agreement has been found between simulations and measurements, indicating the potential of AM LPBF for microwave components in the K_a.

References

[1] L. Manica, P. Rocca, and A. Massa, "On the synthesis of sub-arrayed planar array antennas for tracking radar applications," *IEEE Antennas and Wireless Propagation Letters*, vol. 7, pp. 599–602, 2008.

[2] O. A. Peverini, M. Lumia, G. Addamo, G. Virone, and N. J. G. Fonseca, "How 3D-printing is changing RF front-end design for space applications," *IEEE Journal of Microwaves*, vol. 3, no. 2, pp. 800–814, 2023.

[3] S. Zhang, R. K. Arya, W. G. Whittow, D. Cadman, R. Mittra, and J. C. Vardaxoglou, "Ultra-wideband flat metamaterial grin lenses assisted with additive manufacturing technique," *IEEE Transactions on Antennas and Propagation*, vol. 69, no. 7, pp. 3788–3799, 2021.

[4] J.-M. Poyanco, F. Pizarro, and E. Rajo-Iglesias, "3D-printed integrated grin lens-polarizer using anisotropic materials," *IEEE Transactions on Antennas and Propagation*, pp. 1–1, 2023.

[5] J. Melendro-Jimenez, P. Sanchez-Olivares, A. Tamayo-Dominguez, X. Sun, and J. M. Fernandez-Gonzalez, "3D printed directive beam-steering antenna based on gradient index flat lens with an integrated polarizer for dual circular polarization at w-band," *IEEE Transactions on Antennas and Propagation*, vol. 71, no. 1, pp. 1059–1064, 2023.

[6] O. Zetterstrom, N. J. G. Fonseca, and O. Quevedo-Teruel, "Compact half-Luneburg lens antenna based on a glide-symmetric dielectric structure," *IEEE Antennas Wirel. Propag. Lett.*, vol. 21, no. 11, pp. 2283–2287, 2022.

[7] A. Massaccesi, P. Pirinoli, V. Bertana, G. Scordo, S. L. Marasso, M. Cocuzza, and G. Dassano, "3D-printable dielectric transmitarray with enhanced bandwidth at millimeter-waves," *IEEE Access*, vol. 6, pp. 46 407–46 418, 2018.

[8] S. A. Matos, J. P. Teixeira, J. R. Costa, C. A. Fernandes, N. Nachabe, C. Luxey, D. Titz, F. Gianesello, C. del Rio, A. Arboleya, J.-P. Garnero, and J.-F. Vizzari, "3-D-printed transmit-array antenna for broadband backhaul 5G links at V-band," *IEEE Antennas and Wireless Propagation Letters*, vol. 19, no. 6, pp. 977–981, 2020.

[9] A. F. Vaquero, J. Teixeira, S. A. Matos, M. Arrebola, J. R. Costa, J. M. Felicio, C. A. Fernandes, and N. J. G. Fonseca, "Design of low-profile transmitarray antennas with wide mechanical beam steering at millimeter waves," *IEEE Trans. Antennas Propag.*, vol. 71, no. 4, pp. 3713–3718, 2023.

[10] A. Rebollo, A. F. Vaquero, M. Arrebola, and M. R. Pino, "3D-printed dual-reflector antenna with self-supported dielectric subreflector," *IEEE Access*, vol. 8, pp. 209 091–209 100, 2020.

[11] A. F. Vaquero, A. Rebollo, and M. Arrebola, "Additive manufacturing in compact high-gain wideband antennas operating in mm-wave frequencies," *Sci. Rep.*, 2023.

[12] A. Dorlé *et al.*, "Additive manufacturing of modulated triple-ridge leaky-wave antenna," *IEEE Antennas Wirel. Propag. Lett.*, vol. 17, no. 11, pp. 2123–2127, 2018.

[13] A. Tamayo-Domínguez, J.-M. Fernández-González, and M. Sierra-Castañer, "3-D-printed modified butler matrix based on gap waveguide at w-band for monopulse radar," *IEEE Transactions on Microwave Theory and Techniques*, vol. 68, no. 3, pp. 926–938, 2020.

[14] A. Tamayo-Dominguez, P. Sanchez-Olivares, A. Camacho-Hernandez, and J.-M. Fernandez-Gonzalez, "Guidelines for accurate in-house electroplating and 3-D-printing processes applied to mm-wave devices," *IEEE Microwave and Wireless Components Letters*, vol. 32, no. 11, pp. 1267–1270, 2022.

[15] T. Skaik *et al.*, "Evaluation of 3D printed monolithic G-band waveguide components," *IEEE Trans. Compon. Packaging Manuf. Technol.*, pp. 1–1, 2023.

[16] M. González-Calvo, J. R. Montejo-Garai, J. A. Ruiz-Cruz, and J. M. Rebollar, "Additive manufacturing of a high-performance Q-band circular TE01 mode flared-type transducer," *IEEE Microw. Wirel. Compon. Lett.*, vol. 29, no. 9, pp. 577–579, 2019.

[17] R. Salazar, F. Pizarro, D. Vasquez, and E. Rajo-Iglesias, "Assessment of 3D-printed waveguides using conductive filaments and a chloroform-based smoothing process," *Additive Manufacturing*, vol. 51, p. 102593, 2022.

[18] L. Alonso-González, J. Rico-Fernández, A. F. Vaquero, and M. Arrebola, "Metal-only additive-manufactured in monolithic piece array for sum/difference pattern in Ka-band," *IEEE Trans. Antennas Propag.*, vol. 71, no. 8, pp. 6413–6422, 2023.

[19] P. Castillo-Tapia, J. Rico-Fernández, and O. Quevedo-Teruel, "V-band monolithic additive-manufactured geodesic lens array antenna," *IEEE Antennas Wirel. Propag. Lett.*, vol. 22, no. 10, pp. 2527–2531, 2023.

[20] N. J. G. Fonseca, S.-A. Gomanne, J. Rico-Fernández, P. Jankovic, J. Galdeano, G. Toso, P. Angeletti, M. Arrebola, and O. Quevedo-Teruel, "Fully-metallic additively manufactured monolithic double-ridged waveguide rotman lens in the K/Ka-band," *Sensors*, vol. 23, no. 14, 2023. [Online]. Available: https://www.mdpi.com/1424-8220/23/14/6573

[21] J. Rico-Fernández *et al.*, "Compact and lightweight additive manufactured parallel-plate waveguide half-Luneburg geodesic lens multiple-beam antenna in the K_a-band," *IEEE Antennas Wirel. Propag. Lett.*, vol. 22, no. 4, pp. 684–688, 2023.

[22] C. Silbernagel, I. Ashcroft, P. Dickens, and M. Galea, "Electrical resistivity of additively manufactured AlSi10Mg for use in electric motors," *Additive Manufacturing*, vol. 21, pp. 395–403, 2018.

[23] CST Microwave Studio, *CST Studio Suite*, 2024. [Online]. Available: https://www.cst.com